Chemical and Biomolecular Engineering
2017; 2(1): 19-26
http://www.sciencepublishinggroup.com/j/cbe
doi: 10.11648/j.cbe.20170201.14

Ammonia Decomposition Coupled with Methane Combustion in Catalytic Microreactors for Hydrogen Production

Junjie Chen*, Longfei Yan

Department of Energy and Power Engineering, School of Mechanical and Power Engineering, Henan Polytechnic University, Jiaozuo, China

Email address:
cjjmmm@163.com (Junjie Chen)
*Corresponding author

To cite this article:
Junjie Chen, Longfei Yan. Ammonia Decomposition Coupled with Methane Combustion in Catalytic Microreactors for Hydrogen Production. *Chemical and Biomolecular Engineering.* Vol. 2, No. 1, 2017, pp. 19-26. doi: 10.11648/j.cbe.20170201.14

Received: January 3, 2017; **Accepted**: January 14, 2017; **Published**: February 6, 2017

Abstract: The ammonia decomposition over ruthenium thermally coupled with the catalytic combustion of methane-air mixtures over platinum in catalytic microreactors for hydrogen production was studied numerically, using a two-dimensional computational fluid dynamics model that included detailed chemistry and transport. The effect of flow configuration on the operation characteristics was studied in catalytic microreactors consisting of alternating combustion and decomposition channels separated by a thermally conducting wall. Different performance measures were evaluated to assess the operability of the reactor. It was shown that the high temperatures generated through catalytic combustion result in high conversion in short contact times and thus to compact reactors. Complete conversion of ammonia can be obtained at the micro-scale in both flow configurations. A proper balance of the flow rates of the decomposition and combustion streams is crucial in achieving this. For a given flow rate of combustible mixture, material stability determines the lower power limit, caused by high temperatures generated at low decomposition stream flow rates. In contrast, the maximum power generated is determined by extinction at large decomposition stream flow rates. The two flow configurations were contrasted based on multiple performance criteria, such as reactor temperature, conversion, power exchanged, and hydrogen yield by constructing operating regime. They were found to be practically equivalent for highly conductive materials. Using properly balanced flow rates, the co-current flow configuration expands the operating regime to low and moderate thermal conductivity materials as compared to the counter-current flow configuration that exhibits a slightly superior performance but in a rather narrow operating regime of highly conductive materials and high ammonia flow rates.

Keywords: Catalytic Microreactor, Ammonia Decomposition, Hydrogen Production, Reactor Design, Process Optimization, Catalytic Combustion

1. Introduction

Micro-chemical devices are actively being developed as next generation portable power sources due in part to the superior gravimetric energy density of typical liquid fuels compared to lithium-based batteries [1]. Such a power generation device may consist of a fuel processor, which acts as a hydrogen source, coupled with a proton exchange membrane (PEM) fuel cell. Hydrogen production can be achieved through a number of reactions, i.e., partial oxidation, steam reforming, and auto-thermal reforming of hydrocarbons or alcohols, or cracking of ammonia. Most of these reactions have been carried out in catalytic microreactors. The ammonia decomposition route is particularly attractive for proton exchange membrane fuel cells, as its products are free of carbon monoxide that poisons the fuel cell catalyst and, thus, this route could minimize downstream processing, by eliminating the water-gas shift and the preferential oxidation of carbon monoxide steps [2]. Among these hydrogen production routes, most reactions are endothermic. Therefore, energy must be supplied through an exothermic reaction, such as combustion. The thermal coupling between a combustor and a reformer becomes then an important part of developing stand-alone, multifunctional reactors in which the heat exchange and chemical reaction are coupled in the same device.

The coupling of endothermic and exothermic reactions can be achieved in a number of ways. One strategy is to use "direct" coupling where both reactions are carried out simultaneously in the same reactor using a suitable bi-functional catalyst [3]. A second strategy is "temporal" coupling of the two reactions, where the exothermic and endothermic reactions are alternately carried out in the same reaction chamber [4]. The final heat integration strategy involves "spatial segregation". In this approach, the exothermic and endothermic reactions are carried out in different reaction chambers that are separated by a heat-conducting medium. Spatial segregation allows an independent choice of fuel, of catalysts, and of reaction conditions for the combustor and the reformer. This flexibility in conjunction with the small feature size of a microreactor, which facilitates heat transfer, renders this approach suitable for microreactors [5]. Traditionally, the counter-current mode of heat exchange has a better performance. Recent work has demonstrated an advantage of the co-current flow configuration in lowering catalyst temperature, due to the overlap of reaction zones [6]. However, enhanced transport rates due to small size of microreactors have an impact on the temperature distribution thereby affecting the choice of flow configuration. For example, one can envision nearly isothermal reactors under certain conditions, where co-current and counter-current systems are essentially equivalent. Therefore, the best heat exchange mode at the micro-scale is not obvious and may differ from that of large-scale reactors.

In this study, a spatially segregated mode of the coupling of endothermic and exothermic reactions was investigated in parallel plate catalytic microreactors, using a two-dimensional CFD (computational fluid dynamics) model for co-current and counter-current flow configurations, where ammonia decomposition over ruthenium was coupled with methane catalytic combustion. The latter was chosen to enable high temperatures and complete conversion within short contact times while eliminating problems associated with catalyst deactivation. Furthermore, the effect of flow configuration on operation maps of coupled reactors using various performance measures was explored.

2. Numerical Models and Simulation Approach

2.1. Geometric Model

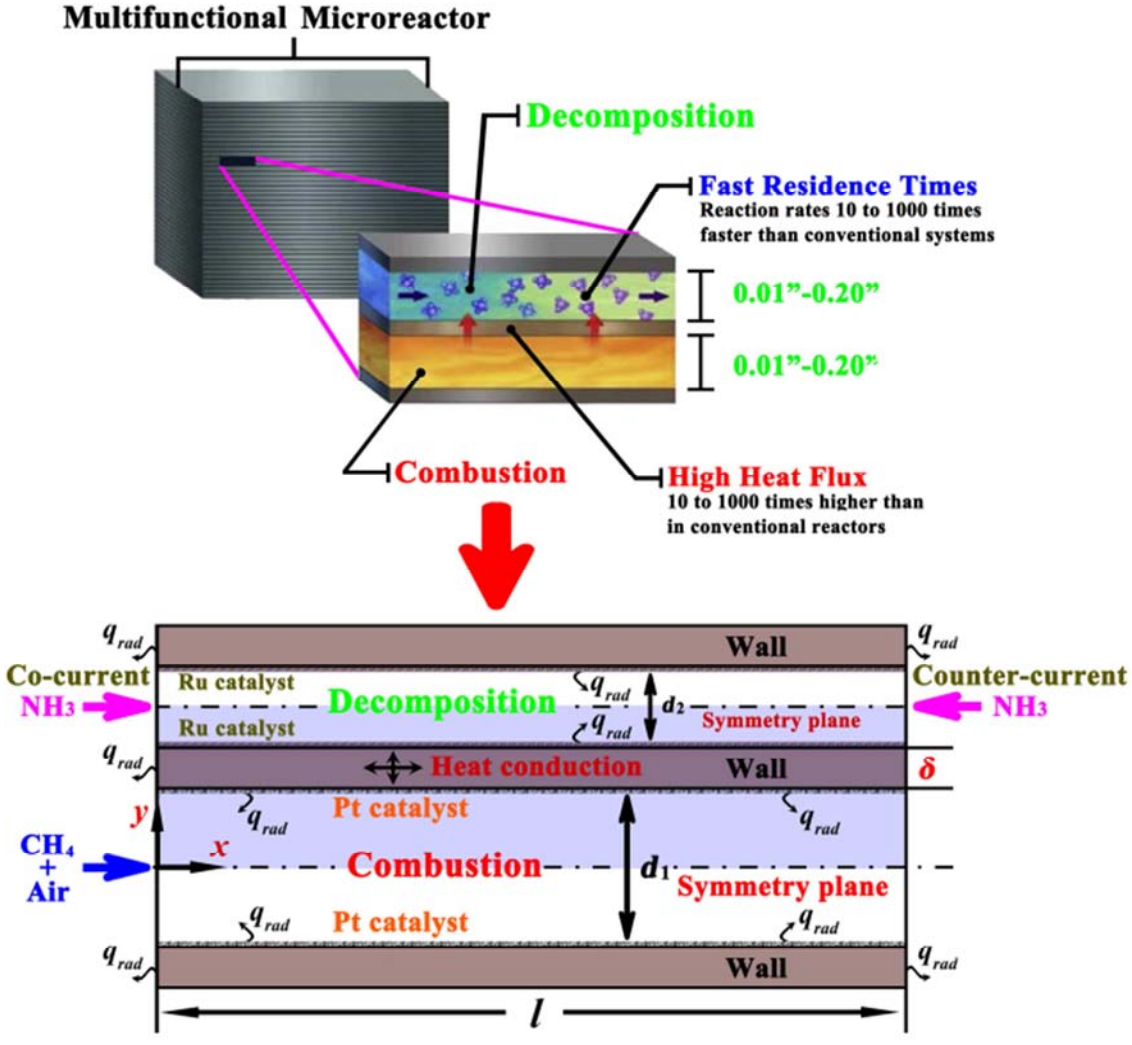

Figure 1. *Schematic diagram of the simulated parallel plate catalytic microreactor with alternating combustion and decomposition channels.*

An integrated parallel plate microreactor geometry is simulated. The combustion and decomposition reactions are carried out in alternate channels separated by walls, as shown schematically in Figure 1. The combustion channel is 0.6 mm wide, the decomposition channel is 0.3 mm wide, and the wall is 0.3 mm thick. The reactor length is 20.0 mm. The stoichiometric methane-air flow in the combustion channel is either co-current or counter-current with respect to the pure ammonia flow in the decomposition channel. Unless otherwise stated, the methane-air inlet flow velocity is 0.8 m/s. Both the fluid streams enter the reactor at ambient temperature and exit at atmospheric pressure. Using the inherent symmetry of the geometry, only one-half of each channel and the connecting wall are simulated. The fluid flow as well as the heat and mass transfer equations are solved in the fluid phase and the energy balance is explicitly accounted for in the solid walls.

2.2. Mathematical Model

The assumptions made are as follows: a steady state is considered; the ideal gas law is assumed; a laminar flow is employed in each channel because the Reynolds number (Re) based on the incoming properties and the channel hydraulic diameters is less than 480; gravity is not considered because it is found to have minimal impact on the computational results for the Reynolds numbers of this study; the radiative heat transfer is considered. A two-dimensional steady state model is employed using the commercial CFD software package ANSYS FLUENT® Release 6.3 [7] incorporates with the detailed homogeneous and heterogeneous reaction schemes in CHEMKIN [8] and Surface-CHEMKIN [9] format to solve the steady state continuity, momentum, energy, and species equations with appropriate boundary conditions. At the vertical wall faces of each parallel plate, both convective and radiative boundary conditions are applied to compute external heat losses. Simple estimates suggest that for the path-lengths and species partial pressures of interest, the gas radiative absorption and emission can be ignored, compared to convection and surface-to-surface radiation. Since the heat recirculation within the wall profoundly affects the combustion stability, the heat conduction within the walls is considered.

2.3. Chemical Kinetics

For the catalytic combustion of methane-air mixtures over platinum, the detailed heterogeneous reaction scheme of Deutschmann *et al*. [10] is employed. A surface site density $\Gamma_{Pt} = 2.72 \times 10^{-9}$ mol/cm^2 is used for the platinum catalyst [10]. For the ammonia decomposition over ruthenium, the detailed heterogeneous reaction scheme of Deshmukh *et al*. [11] is employed. A surface site density $\Gamma_{Ni} = 2.90 \times 10^{-9}$ mol/cm^2 is used for the ruthenium catalyst [11]. The computational tool DETCHEM [12] is applied to treat the problem numerically. Gaseous and surface thermodynamic data are included in the provided schemes. Mixture-average diffusion coefficients are used in conjunction with the CHEMKIN transport database [13].

2.4. Computation Scheme

The fluid density is computed using the ideal gas law. The individual properties of various gaseous species, such as thermal conductivity, are computed using the kinetic theory of gases, whereas the specific heats are determined as a function of temperature using polynomial fits [14]. Mixture properties, such as thermal conductivity and specific heat, are computed from pure component values based on the mass-fraction weighted mixing law [15]. Binary species diffusivities are determined using the Chapman-Enskog equation and then are used to compute the multicomponent mixture diffusivities. For the solid wall, a constant specific heat and an isotropic thermal conductivity are specified. Given that material thermal conductivity varies with temperature and more importantly with the material chosen, simulations are carried out over a wide range of wall thermal conductivities.

The model boundary conditions are described as follows. Danckwerts boundary conditions are implemented for the species and temperatures at the inlets to better mimic experimental conditions [16]. Both gases enter the channels at ambient temperature with a uniform, flat flow velocity. The reactor exits are held at a fixed atmospheric pressure and the normal gradients of species and temperature, with respect to the direction of the flow, are set to zero. Symmetry boundary condition is applied at the centerline of both channels, implying a zero normal velocity and zero normal gradients of all variables. No-slip boundary condition is applied at each wall-fluid interface. Continuity in temperature and heat flux is applied at the fluid-solid interfaces. It should be noted that neither heat-transfer nor mass-transfer correlations are employed since detailed transport within the solid and fluid phases is explicitly accounted for. The full problem is solved through a segregated solver using an under-relaxation method. Convergence of the solution is monitored through the residuals of the governing equations. The solution is deemed converged when the residuals of the equations are less than 10^{-6}. Parallel processing using a message passing interface (MPI) is used to speed up the most demanding computations. Natural parameter continuation is employed to study the effect of various operating parameters.

In order to verify the numerical scheme implemented in the present work, the experimental results of Ganley *et al*. [17] are utilized. In their work, a ruthenium-impregnated anodic aluminum catalyst is used in microreactors for the production of hydrogen from an ammonia feed. The predictions for the operating conditions are in good agreement with the experimental microreactor data, without tuning of any of the reaction parameters (data not shown).

3. Results and Discussion

The material stability in terms of maximum allowable wall temperature is the first important operating criterion. Lower

wall temperatures are essential for the stability of catalyst and construction material. Lower reactor temperatures are essential for the stability of catalyst and construction materials employed in the ammonia decomposition channel. A maximum wall temperature of 1500 K is selected as a reasonable, albeit arbitrary, limit for stability of catalyst and reactor structural material (hereafter termed as materials stability limit), i.e., wall and catalyst temperatures in excess of this value are deemed detrimental to the reactor. Note that the melting point of ruthenium is 2607 K, and the melting point of platinum is 2042 K, which is about 560 K less than that of ruthenium. The choice of the temperature threshold defined here stems from similar temperatures observed in short contact time reactors, in which noble metal catalysts (e.g. platinum, rhodium, nickel, palladium, and iridium) have been found to be stable up to temperatures of 1500 K [18]. Additionally, ruthenium catalysts have been used for steam reforming of methane and found to be stable for periods of 100 hours tested [19]. The material stability determines the lower power output limit for a given combustible stream flow rate.

3.1. Effect of Wall Thermal Conductivity

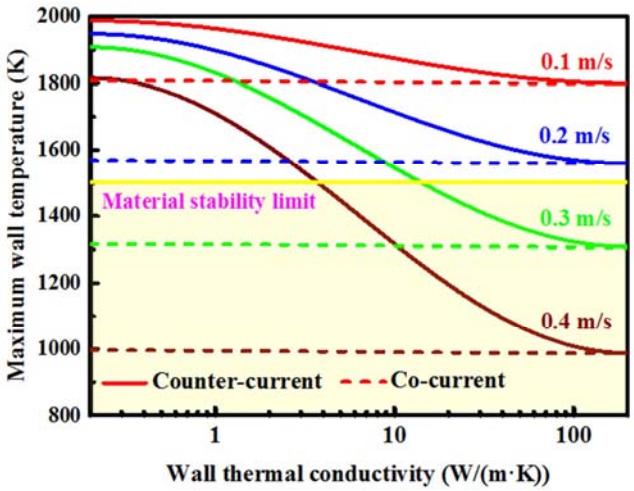

Figure 2. *Effect of wall thermal conductivity on the maximum wall temperature. The shaded region indicates the material stability limit.*

The wall thermal conductivity is an important parameter which determines the reactor stability. Therefore, it is important to exploit the effect of the construction material of reactors. For comparison purposes, simulations are performed for different wall thermal conductivities in the range of 0.2-200 W/(m·K). Although some very conductive materials (e.g., aluminum and copper) have higher thermal conductivities, the results discussed herein do not differ for wall thermal conductivities higher than 200 W/(m·K). Figure 2 shows the effect of wall thermal conductivity on the maximum wall temperature at various ammonia inlet flow velocities. For highly conductive materials, the temperature profiles of the two flow configurations are nearly identical. The high wall thermal conductivity implies rapid heat conduction that results in nearly isothermal wall temperatures. In this case, the time-scale of wall heat conduction is much smaller than the residence time rendering the effect of flow configuration secondary. However, with the decrease of wall thermal conductivity, differences between the two flow configurations emerge. In the counter-current flow configuration, the heat generation and heat removal are separated by the length of the reactor, and a low wall thermal conductivity implies slow heat transfer resulting in very hot walls near the combustion zone. In addition, significant temperature gradients may occur within the wall. Almost identical behavior of the two flow configurations is observed for high thermal conductivity materials. The maximum temperature of a co-currently coupled reactor is nearly independent of wall thermal conductivity, whereas a counter-currently coupled reactor exhibits very high wall temperatures at lower wall thermal conductivities. The shaded region demarcates the operating regime of allowable reactor temperatures. Co-current operation results in lower reactor temperatures and allows a wider choice of materials than that of the counter-current flow configuration.

3.2. Power Exchanged

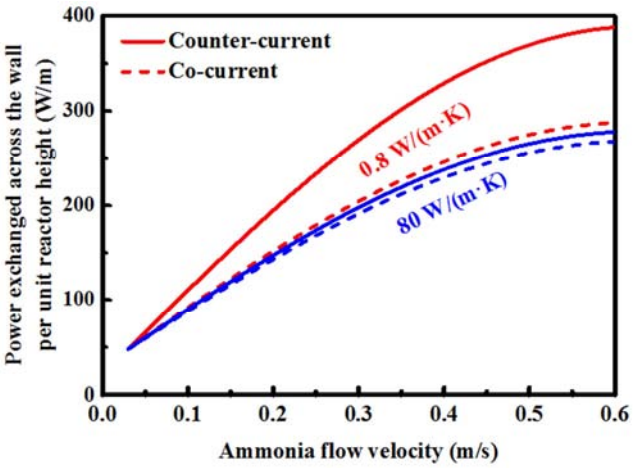

Figure 3. *Effect of ammonia flow velocity on the power exchanged across the wall per unit reactor height for select wall thermal conductivities.*

The power exchanged across the wall is an important performance measure since a primary objective of a multifunctional reactor is to maximize the heat exchange between the two reaction zones. Previously, the critical power removed at extinction has been used as a stability criterion for gaseous micro-combustors [20]. Figure 3 shows the power exchanged per unit height of the reactor as a function of ammonia flow rate for different wall thermal conductivities. The end points of the curves at high ammonia flow rates correspond to the critical power exchanged prior to extinction. In the co-current flow configuration, the power exchanged is practically independent of the material chosen. On the other hand, a strong dependence of the power transferred on the wall thermal conductivity can be observed in the counter-current flow configuration, especially at high ammonia flow rates. The powers exchanged in the two flow

configurations become practically equal for highly conductive materials, corresponding to metals and high conductivity ceramics, where the time-scale of axial heat conduction is so short that heat transfer is independent of the flow configuration. At the other extreme of low wall thermal conductivity, the time-scale of transverse heat conduction becomes larger than the residence time rendering the effect of flow configuration small. However, for moderate wall thermal conductivities, there is a competition between the heat conduction time-scale and flow residence time, and therefore, the flow configuration plays a role in heat exchange. In particular, the power exchanged in the counter-current flow configuration is larger for moderate conductive materials. Materials in this conductivity range, corresponding to high temperature ceramics such as alumina and silica, have previously been used for the fabrication of micro-combustors [21] and have been reported to be most stable to heat losses [22]. Therefore, the two flow configurations show nearly identical performance at the extremes of material conductivity range in terms of the power exchanged, but the counter-current flow configuration is better for moderate wall thermal conductivities.

3.3. Exit gas Temperature

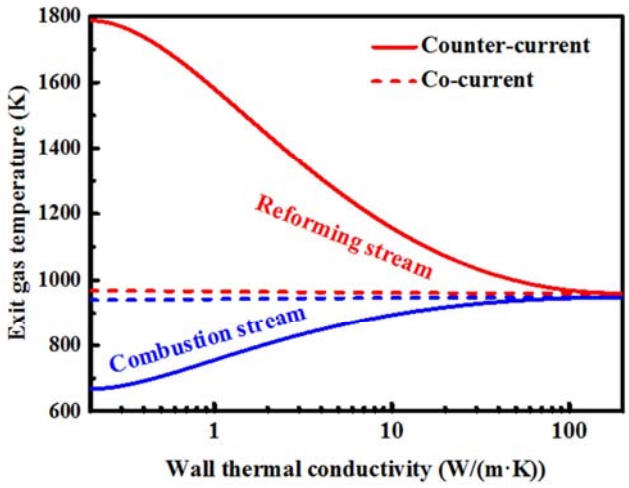

Figure 4. *Effect of wall thermal conductivity on the exit gas temperatures.*

Figure 4 shows the exit gas temperatures as a function of wall thermal conductivity. The ammonia inlet flow velocity is 0.8 m/s. In the counter-current flow configuration, the larger power exchanged comes at the cost of larger maximum wall temperature, higher exit temperature of the decomposition stream, as it flows past the hot combustion zone, and a lower combustion stream exit temperature. High temperatures of the decomposition stream are undesirable for proton exchange membrane fuel cell applications where the stream has to be cooled down to about 360 K [23]. Note that the proton exchange membrane fuel cell is a promising alternative power source for various applications in portable power device, vehicles, and stationary power plants [24]. Therefore, a comparison in terms of the critical power exchanged may be misleading and thus not a good performance criterion for integrated reactors producing hydrogen. These numerical results indicate the rather expected outcome that optimizing individual components, e.g., a combustor and a reformer, is not necessarily a good strategy for developing design principles for coupled reactors.

3.4. Hydrogen Production

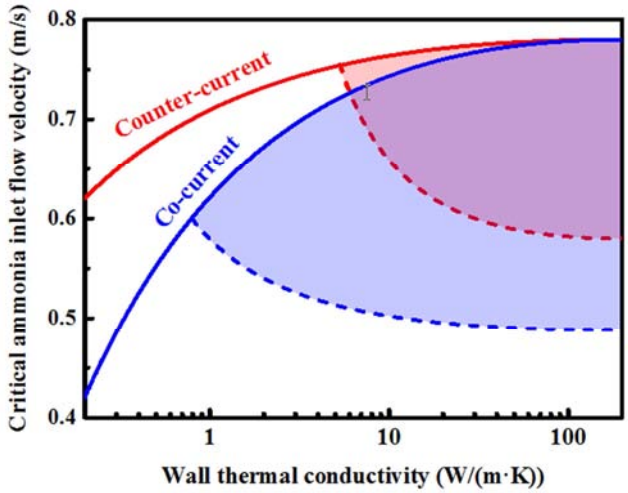

Figure 5. *Effect of wall thermal conductivity on the critical ammonia inlet flow velocity. The shaded region demarcates the operating regime delimited by extinction and material stability.*

The hydrogen flow rate is perhaps the most important performance measure of an integrated reactor. It depends not only on the ammonia flow rate but also on the ammonia conversion. Figure 5 shows the critical ammonia inlet flow velocity as a function of wall thermal conductivity. The critical ammonia inlet flow velocity corresponds to extinction. For a given wall thermal conductivity, any ammonia inlet flow velocity above the critical one, i.e., above the line connecting the points cannot be self-sustained. Therefore, operation is limited below the line of each flow configuration. Larger wall thermal conductivities result in increased heat recirculation and therefore aid in stabilizing higher ammonia flow rates, irrespective of the flow configuration. The overlap of reaction zones in the co-current flow configuration results in diminished stability of the reactor, i.e., lower maximum ammonia flow velocities, especially for highly insulating materials. However, the difference in stability between the two flow configurations becomes less pronounced for highly conductive materials. Given that low ammonia flow rates result in high wall temperatures, the shaded areas indicate a coarse operating regime of realizable flows and wall materials. The upper boundary of flow is determined from extinction, whereas the lower boundary of flow and wall thermal conductivity from the material stability limit. The materials limit criterion renders the counter-current flow configuration only slightly better for a narrow range of materials. It is clear that the co-current flow configuration allows a wider choice of wall materials.

3.5. Maximum Power Generated

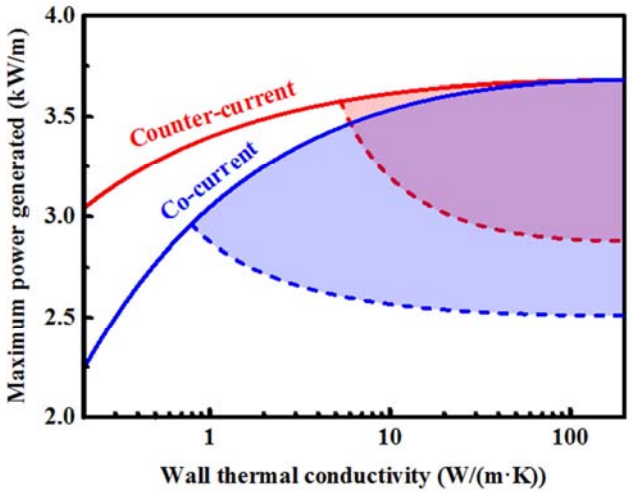

Figure 6. *Effect of wall thermal conductivity on the maximum power generated based on the hydrogen produced. The shaded region demarcates the operating regime delimited by extinction and material stability.*

The maximum power generated corresponds to the maximum hydrogen yield. Depending on the overall process flow sheet, operation with the maximum power generated may be desirable. Figure 6 shows the maximum power generated per unit reactor height from the hydrogen produced as a function of wall thermal conductivity. The maximum power generated accounts for both the critical ammonia flow rate and the ammonia conversion, assuming 100% fuel cell efficiency. The shaded region demarcates again the operating regime delimited by extinction and material stability. Due to the high conversions under reasonable operating conditions, the similar features of the critical ammonia inlet flow velocity can be obtained. The counter-current operation is slightly better in a narrow operating regime. The co-current flow configuration allows a wider choice of fabrication materials and catalysts.

3.6. Operation Map

In this section, operation maps are presented in order to guide the design of integrated reactors based on a projected power requirement. While these operation maps clearly pertain to parallel plate geometries of fixed dimensions and to the specific fuels, the approach employed herein is general and similar findings are expected for other multifunctional micro-chemical devices. A 100% fuel cell efficiency is assumed in all computations, given that a lower efficiency would scale the results exactly proportionally. Based on the discussion above, only a narrow range of powers can be achieved for a fixed methane-air flow rate. The minimum power is determined from the lowest allowable ammonia flow rate that in turn is dictated by the material limit set at 1500 K. The maximum power corresponds to the critical value prior to extinction. The minimum power generated corresponds to the co-current flow configuration, whereas the maximum power generated corresponds to the counter-current flow configuration at high wall thermal conductivities. Powers outside this range cannot be achieved irrespective of the flow configuration or wall material chosen. One could envisage a "scale-out" type of approach [25], using multiple units in parallel, to achieve higher powers or changing the reactor dimensions to enable lower powers, while keeping the residence time constant [26]. It should be noted that the computed powers are dependent on the choice of fuel. However, given a single reactor consisting of two channels only with fixed channel length, operation outside this power range without changing the fuel implies varying the methane-air flow rates.

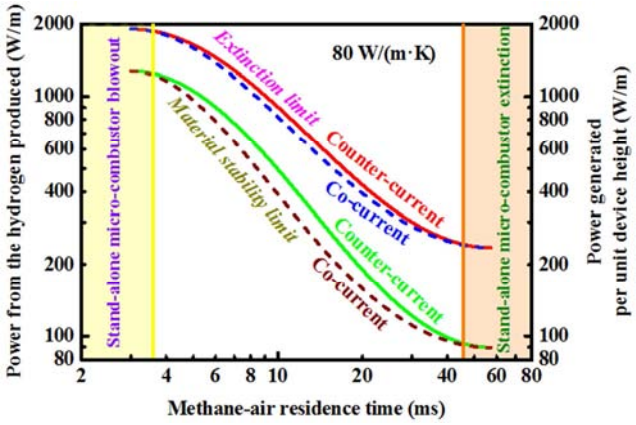

Figure 7. *Operation map indicating the power generated based on the hydrogen produced as a function of methane-air residence time. The vertical shaded areas indicate those for a stand-alone micro-combustor.*

The fuel-air residence times in micro-combustors have been found to be restricted to a finite operating regime for self-sustained combustion [27]. Very fast fuel-air flows cause blowout, given that the residence time is not long enough for self-sustained operation to be possible; in contrast, very slow flows result in extinction, since not enough heat is produced to keep up with the heat loss to the surroundings [28]. A two parameter continuation is used to track the power generation as a function of the ammonia flow rate for various methane-air residence times. Figure 7 shows the operation map indicating the power generated based on the hydrogen produced as a function of methane-air residence time. A 100% fuel cell efficiency is assumed. The shaded vertical rectangles provide an idea of the residence time limits. The limits of the operating regime depend on the choice of flow configuration as well as the wall material. High wall thermal conductivity represents the maximum power produced and also results in an equivalent performance of the two flow configurations. Therefore, the counter-current flow configuration with a high wall thermal conductivity of 80 W/(m·K) is chosen for the majority of runs and CFD simulations are performed for different methane-air residence times. A narrow operating regime is achieved, as indicated by the cross-hatched area. For both flow configurations and all methane-air residence times, an upper bound for the power is caused by the critical ammonia inlet flow velocity, whereas the lower bound depicts the material limit in terms of the reactor temperature. A balance between the methane-air and ammonia flow rates is crucial in enabling self-sustained operation of a coupled

microreactor. Stable operation outside the methane-air residence time regime predicted by CFD simulations of the stand-alone micro-combustor is also an evidence of the enhanced stability of the integrated reactor. The power generation plots can be used as a guide in designing integrated microreactors. One can select a desired power, and trace it to the operating regime to estimate the required methane-air residence time.

4. Conclusions

The ammonia decomposition over ruthenium thermally coupled with the catalytic combustion of methane-air mixtures over platinum in catalytic microreactors for hydrogen production was studied numerically. Computations were carried out using a two-dimensional CFD model that included detailed chemistry and transport. Two flow configurations, i.e., co-current and counter-current, were contrasted in terms of various performance criteria including reactor temperatures, temperature of exit gas stream, maximum power exchanged, and hydrogen production achieved. For any combustible flow rate, the operating regime of a microreactor is delimited by extinction caused from fast ammonia flows and by material stability, in terms of reasonable reactor temperatures, at sufficiently slow ammonia flows.

For highly conductive materials, the co-current and counter-current flow configurations behave similarly in all performance measures simply because high wall thermal conductivity coupled with small reactor scales renders the operation nearly isothermal. The co-current flow configuration enables lower reactor temperatures and a wider spectrum of materials to be used, whereas the counter-current flow configuration shows superior performance albeit in a very narrow operating regime of high ammonia flow rates and highly conductive materials. Since this advantage of the counter-current flow configuration is only slight, the co-current flow configuration should be preferred for actual reactors.

Finally, while the catalytic combustion of fuel-air mixtures can lead to result in high temperatures and drive ammonia decomposition to completion in milliseconds, meanwhile it results in a relatively narrow range of balanced flow rates in order to prevent material stability and avoid extinction issues. Future work will explore the use of alternative coupling modes and chemistries in order to broaden the operation regime.

Acknowledgement

This work was supported by the National Natural Science Foundation of China (No. 51506048).

References

[1] J. D. Holladay and Y. Wang. A review of recent advances in numerical simulations of microscale fuel processor for hydrogen production. *Journal of Power Sources*, Volume 282, 2015, Pages 602-621.

[2] V. R. Regatte and N. S. Kaisare. Hydrogen generation in spatially coupled cross-flow microreactors. *Chemical Engineering Journal*, Volumes 215-216, 2013, Pages 876-885.

[3] R. C. Ramaswamy, P. A. Ramachandran, and M. P. Duduković. Recuperative coupling of exothermic and endothermic reactions. *Chemical Engineering Science*, Volume 61, Issue 2, 2006, Pages 459-472.

[4] G. Kolios, J. Frauhammer, and G. Eigenberger. Autothermal fixed-bed reactor concepts. *Chemical Engineering Science*, Volume 55, Issue 24, 2000, Pages 5945-5967.

[5] G. D. Stefanidis and D. G. Vlachos. High vs. low temperature reforming for hydrogen production via microtechnology. *Chemical Engineering Science*, Volume 64, Issue 23, 2009, Pages 4856-4865.

[6] S. R. Deshmukh and D. G. Vlachos. Effect of flow configuration on the operation of coupled combustor/reformer microdevices for hydrogen production. *Chemical Engineering Science*, Volume 60, Issue 21, 2005, Pages 5718-5728.

[7] *Fluent 6.3 user's guide*. Lebanon, New Hampshire: Fluent Inc., 2006.

[8] R. J. Kee, F. M. Rupley, E. Meeks, and J. A. Miller. *CHEMKIN-III: a Fortran chemical kinetics package for the analysis of gasphase chemical and plasma kinetics*, Report No. SAND96-8216, Sandia National Laboratories, 1996.

[9] M. E. Coltrin, R. J. Kee, F. M. Rupley, and E. Meeks. *SURFACE CHEMKIN-III: a Fortran package for analyzing heterogeneous chemical kinetics at a solid-surface-gas-phase interface*, Report No. SAND96-8217, Sandia National Laboratories, 1996.

[10] O. Deutschmann, L. I. Maier, U. Riedel, A. H. Stroemman, and R. W. Dibble. Hydrogen assisted catalytic combustion of methane on platinum. *Catalysis Today*, Volume 59, Issues 1-2, 2000, Pages 141-150.

[11] S. R. Deshmukh, A. B. Mhadeshwar, and D. G. Vlachos. Microreactor modeling for hydrogen production from ammonia decomposition on ruthenium. *Industrial & Engineering Chemistry Research*, Volume 43, Issue 12, 2004, Pages 2986-2999.

[12] O. Deutschmann, S. Tischer, C. Correa, D. Chatterjee, S. Kleditzsch, V. M. Janardhanan, N. Mladenov, H. D. Minh, H. Karadeniz, and M. Hettel, *DETCHEM Software package*, 2.5 Edition, www.detchem.com, Karlsruhe, 2014.

[13] R. J. Kee, G. Dixon-lewis, J. Warnatz, M. E. Coltrin, J. A. Miller, and H. K. Moffat. *A Fortran computer code package for the evaluation of gas-phase, multicomponent transport properties*, Report No. SAND86-8246B, Sandia National Laboratories, 1998.

[14] D. G. Norton and D. G. Vlachos. Combustion characteristics and flame stability at the microscale: a CFD study of premixed methane/air mixtures. *Chemical Engineering Science*, Volume 58, Issue 21, 2003, Pages 4871-4882.

[15] D. G. Norton and D. G. Vlachos. A CFD study of propane/air microflame stability. *Combustion and Flame*, Volume 138, Issues 1-2, 2004, Pages 97-107.

[16] R. Sui and J. Mantzaras. Combustion stability and hetero-/homogeneous chemistry interactions for fuel-lean hydrogen/air mixtures in platinum-coated microchannels. *Combustion and Flame*, Volume 173, 2016, Pages 370-386.

[17] J. C. Ganley, E. G. Seebauer, and R. I. Masel. Porous anodic alumina microreactors for production of hydrogen from ammonia. *AIChE Journal*, Volume 50, Issue 4, 2004, Pages 829-834.

[18] P. M. Torniainen, X. Chu, and L. D. Schmidt. Comparison of monolith-supported metals for the direct oxidation of methane to syngas. *Journal of Catalysis*, Volume 146, Issue 1, 1994, Pages 1-10.

[19] A. Berman, R. K. Karn, and M. Epstein. Kinetics of steam reforming of methane on Ru/Al_2O_3 catalyst promoted with Mn oxides. *Applied Catalysis A: General*, Volume 282, Issues 1-2, 2005, Pages 73-83.

[20] N. S. Kaisare and D. G. Vlachos. Optimal reactor dimensions for homogeneous combustion in small channels. *Catalysis Today*, Volume 120, Issue 1, 2007, Pages 96-106.

[21] C. M. Miesse, R. I. Masel, C. D. Jensen, M. A. Shannon, and M. Short. Submillimeter-scale combustion. *AIChE Journal*, Volume 50, Issue 12, 2004, Pages 3206-3214.

[22] N. S. Kaisare, S. R. Deshmukh, and D. G. Vlachos. Stability and performance of catalytic microreactors: Simulations of propane catalytic combustion on Pt. *Chemical Engineering Science*, Volume 63, Issue 4, 2008, Pages 1098-1116.

[23] N. Djilali. Computational modelling of polymer electrolyte membrane (PEM) fuel cells: Challenges and opportunities. *Energy*, Volume 32, Issue 4, 2007, Pages 269-280.

[24] H.-W. Wu. A review of recent development: Transport and performance modeling of PEM fuel cells. *Applied Energy*, Volume 165, 2016, Pages 81-106.

[25] M. S. Mettler, G. D. Stefanidis, and D. G. Vlachos. Enhancing stability in parallel plate microreactor stacks for syngas production. *Chemical Engineering Science*, Volume 66, Issue 6, 2011, Pages 1051-1059.

[26] G. D. Stefanidis and D. G. Vlachos. Millisecond methane steam reforming via process and catalyst intensification. *Chemical Engineering & Technology*, Volume 31, Issue 8, 2008, Pages 1201-1209.

[27] J. Wan, A. Fan, and H. Yao. Effect of the length of a plate flame holder on flame blowout limit in a micro-combustor with preheating channels. *Combustion and Flame*, Volume 170, 2016, Pages 53-62.

[28] Y. Yan, W. Huang, W. Tang, L. Zhang, L. Li, J. Ran, and Z. Yang. Numerical study on catalytic combustion and extinction characteristics of pre-mixed methane-air in micro flatbed channel under different parameters of operation and wall. *Fuel*, Volume 180, 2016, Pages 659-667.